

Available online at [www.sciencedirect.com](http://www.sciencedirect.com)

**jmr&t**  
Journal of Materials Research and Technology  
journal homepage: [www.elsevier.com/locate/jmrt](http://www.elsevier.com/locate/jmrt)



## Original Article

# The effect of flux chemistry on element transfer in Submerged Arc Welding: application of thermochemical modelling



T. Coetsee <sup>a,\*</sup>, R.J. Mostert <sup>a</sup>, P.G.H. Pistorius <sup>a</sup>, P.C. Pistorius <sup>b</sup>

<sup>a</sup> Department of Materials Science and Metallurgical Engineering, University of Pretoria, Pretoria, 0002, South Africa

<sup>b</sup> Carnegie Mellon University, Pittsburgh, PA, USA

## ARTICLE INFO

## Article history:

Received 12 October 2020

Accepted 10 February 2021

Available online 18 February 2021

## Keywords:

FactSage

Welding

Slag

Fluoride

Flux

Steel

## ABSTRACT

Post-weld slag and weld metal analyses were used to interpret the effects of different commercial flux compositions on element transfer between molten flux (slag) and weld metal in Submerged Arc Welding (SAW). Selected fluoride based flux compositions cover a wide range of basicity index (BI) values of 0.5–3.0. Thermochemical modelling in FactSage software is used to simulate the welding process in terms of gas-slag-metal equilibria. The importance of the gas phase in SAW element transfer is illustrated. The model provides improved accuracy in predicted weld metal oxygen values (ppm O) compared to the generally used empirical relationship of weld metal ppm O vs. flux BI. Model predicted oxygen values are within 150 ppm of the analysed values, compared to the empirical relationship values which are within 240 ppm from the analysed values. The model provides resolution in ppm O values at BI > 1.8. This information is lacking in the empirical relationship with constant ppm O of 250 ppm at BI > 1.8. The measured ppm O values follow the Fe–FeO equilibrium trend with a positive offset. The relative level of oxygen to deoxidation elements (Ti, Al, Mn, Si) in the weld metal is an important factor in oxide inclusion engineering. This model will aid in the specification of flux formulations to attain specific weld metal compositions for maximum acicular ferrite formation. In this way the weld metal mechanical properties can be improved. This model will reduce the number of welding tests required to develop new flux formulations.

© 2021 The Author(s). Published by Elsevier B.V. This is an open access article under the CC BY-NC-ND license (<http://creativecommons.org/licenses/by-nc-nd/4.0/>).

## 1. Introduction

Submerged Arc Welding (SAW) has an extensive history of industrial application and research, spanning more than 100 years [1]. The SAW process allows for efficient welding of thick

steel plates in heavy engineering industries such as ship-building and pressure vessel construction [1]. In the SAW process, electrical and chemical parameters are combined to form an arc between the weld wire tip and the steel base plate. Raw unmelted flux (flux) and molten flux (slag) cover the arc to

\* Corresponding author.

E-mail address: [theresa.coetsee@up.ac.za](mailto:theresa.coetsee@up.ac.za) (T. Coetsee).

<https://doi.org/10.1016/j.jmrt.2021.02.046>

2238-7854/© 2021 The Author(s). Published by Elsevier B.V. This is an open access article under the CC BY-NC-ND license (<http://creativecommons.org/licenses/by-nc-nd/4.0/>).

form the arc cavity. The covered arc ensures high heat transfer efficiency in SAW, compared to open arc welding methods [1]. Weld wire and flux are continuously fed through the welding head arrangement as it moves along the weld. In the arc cavity the molten weld wire metal droplets are transferred into the weld pool as complex physical and chemical interactions of heat and mass transfer occur [1,2]. Chemical reactions continue in the trailing molten weld pool of slag and steel, until the steel is solidified as weld metal [3,4].

The welded steel composition is influenced by applied welding parameters of voltage, current, polarity, and welding speed, and by slag-steel-gas chemical reactions in the weld pool and arc cavity [3–6]. Weld pool reaction time is set by heat input, itself a combination of voltage, current and welding speed [7]. Welding studies are typically focused on analysis of the weld metal chemistry, and the particular mechanical properties attained from using specific flux formulations. There is less research focus on the metallurgical process of element transfer from the slag to the weld metal [8–11].

Despite the high importance of welding parameters in SAW, the weld metal chemistry is mostly set by the flux composition via setting of the oxygen potential in the arc cavity [5,12]. Flux compositions are designed to attain targeted weld metal chemistries through element transfer between the slag and the weld metal. Slags must also exhibit specific physico-chemical properties to facilitate the SAW process. Examples of these properties are flux composition design to

An important empirically determined flux composition guideline is to ensure that the flux BI is in excess of 1.5 to ensure low hydrogen and low total oxygen content in the weld metal [14,24]. Weld metal oxygen must be controlled within a relatively narrow band to ensure high weld metal impact toughness. Both too low (<200 ppm O) and too high (>500 ppm) weld metal oxygen were found to be detrimental to weld metal impact toughness [8]. Oxide inclusion engineering is used to enhance acicular ferrite phase formation in the weld metal, which ensures an increase in weld metal impact toughness [8,23–25]. The oxide inclusion phase distribution, inclusion size and inclusion element stoichiometry are influenced by the concentration ratio of deoxidising element to oxygen in the steel, for example [Ti]/[O] or [Al]/[O] in the weld metal [6,7,27–29]. It was shown that a 100% CaF<sub>2</sub> flux lowers weld metal oxygen since no oxygen is introduced into the weld metal when there are no oxides contained in the flux [8]. Similarly, addition of CaF<sub>2</sub> to an oxide containing flux lowers weld metal oxygen as the CaF<sub>2</sub> addition dilutes oxides in the flux [20]. Most of the flux CaF<sub>2</sub> ends up in the slag as CaF<sub>2</sub> to perform all its above mentioned functions. Therefore it is important to include this compound in the BI expression [8]. Eq. (1) was originally defined as the ratio of network breaker to network former compounds, each expressed in mass% [24]. Eq. (1) is an extension of the simple B3 basicity of (mass% CaO + mass% MgO)/(mass% SiO<sub>2</sub>) used for pyrometallurgical slags by adding the compounds typically present in SAW flux.

$$BI = \frac{\%CaF_2 + \%CaO + \%MgO + \%BaO + \%SrO + \%Na_2O + \%K_2O + \%Li_2O + 0.5(\%MnO + \%FeO)}{\%SiO_2 + 0.5(\%Al_2O_3 + \%TiO_2 + \%ZrO_2)} \quad (1)$$

ensure optimum levels of slag viscosity and surface tension to sufficiently shield the weld pool from atmospheric gasses; and to ensure that the slag liquidus temperature is 50 °C lower than the weld metal solidification temperature [5,6,13].

Most SAW fluxes contain some quantity of CaF<sub>2</sub> to reduce weld metal hydrogen content by shielding the weld pool from atmospheric air, to increase the slag hydrogen dissolution capacity, and to react with water to form hydrogen fluoride gas [14,18,20,22,23]. In addition to these reasons for adding CaF<sub>2</sub> to fluxes, the important chemical action of CaF<sub>2</sub> is to lower slag melting temperatures significantly and to serve as a slag network modifier to lower slag viscosity and surface tension. CaF<sub>2</sub> additions may also influence plasma arc phenomena. Increased CaF<sub>2</sub> additions to the flux decrease the arc length by decreasing plasma conductivity due to an increase in the ratio of fluorine to oxygen in the arc cavity [1]. CaF<sub>2</sub> additions increase the slag electrical conductivity, and excessive CaF<sub>2</sub> additions may cause current loss to the slag shell [1]. Despite the clear importance of CaF<sub>2</sub> in flux formulations, its role in weld slag chemistry is complex. For example, it was argued that CaF<sub>2</sub> should be removed as a basic flux compound in the widely used flux basicity index (BI) in Eq. (1). This equation is generally used in SAW flux chemistry specifications [3,8]. The reasoning for its exclusion was that CaF<sub>2</sub> is a chemically neutral slag compound [1,20].

The SiO<sub>2</sub> and MnO additions to flux formulations are made to control Si and Mn levels in the weld metal of low alloy carbon steels. Flux element transfer behaviour is often described as neutral in Si and/or Mn alloying, to low, moderately or high alloying in Si and/or Mn alloying. Addition of CaO is avoided in agglomerated fluxes because it is hygroscopic [20]. Instead the CaO may be added as CaCO<sub>3</sub>, but only in limited quantities because the CO<sub>2</sub> from carbonate decomposition is a source of oxygen in the plasma arc [3,18,20]. In fused (premelting) fluxes the hygroscopic effect of CaO is avoided because CaO forms part of the slag structure. Binary CaF<sub>2</sub>-oxide flux formulations used in SAW, under Ar atmosphere, confirmed the plasma arc stability order of the oxides from high to low stability: CaO, K<sub>2</sub>O, Na<sub>2</sub>O and TiO<sub>2</sub>, Al<sub>2</sub>O<sub>3</sub>, MgO, SiO<sub>2</sub> and MnO [20]. Alkali metal oxides (K<sub>2</sub>O and Na<sub>2</sub>O) may be added to stabilise the arc [10]. Although Eq. (1) displays FeO, it is mostly absent from flux formulations or limited to less than two mass% [3].

It is well established that the weld carbon content changes very little from the nominal composition, calculated as the expected weld metal composition from the proportions of weld wire and base plate metal welded into the weld metal [6,35]. It was stated that FeO, which is typically limited to less than two mass% in welding flux, does not significantly affect

**Table 1 – Plate and wire compositions (mass%).**

	C	O	Si	Mn	Al	P	S	Ti	Cu
Plate	0.120	0.007	0.155	1.340	0.067	0.019	0.007	0.005	0.030
Wire	0.110	0.003	0.137	0.990		0.009	0.023		0.140

weld metal oxygen content [3]. However, the weld metal total oxygen content increased with increased FeO in the flux in the SiO<sub>2</sub>–MnO–FeO system [16]. In this study, the SiO<sub>2</sub> level was kept constant at 40 mass% SiO<sub>2</sub>, and the less stable FeO was replaced for more stable MnO in the flux [16].

Development of predictive models of the weld metal chemical composition requires a control data set to test the quality of model outputs [14]. A limited number of published studies reported post-weld slag compositions and/or slag properties for SAW, or even for similar welding techniques [15–19,33,34]. Several studies used slag-steel equilibrium calculations as the basis for explaining the effect of flux composition on element transfer between the slag and the weld metal [3,14–16,21]. Differences between the analysed weld metal composition and the predicted equilibrium values were explained to be due to uncertainty in the accuracy of the equilibrium calculation temperature used to simulate the weld pool reactions, the importance of kinetic factors in reactions, and the importance of the plasma arc reactions in setting slag pool chemistry [3,6]. An extensive model was developed to account for these effects by incorporating kinetic parameters, slag-metal equilibrium calculations and physical geometric parameters represented by the slag-metal interface area and weld metal volume [6]. However, such a model requires extensive empirical inputs from welding tests. None of these models calculated the weld metal ppm O. Instead, the empirical relationship of flux BI vs. ppm O in the weld metal, established by Tuliani et al. [24], was used to set the weld metal ppm O level as the starting point of equilibrium calculations.

In thermodynamic calculations, the level of oxygen available within the weld pool sets the element distribution between slag and metal because of the relative difference in oxygen affinity of the steel alloying elements [14]. Previous studies have shown that the main uncertainty in equilibrium calculations for weld metal compositions is the effect of large quantities of oxygen introduced from flux and gas [6,14,20]. Excessive levels of oxygen is initially added to the molten weld wire droplets from the arc cavity gas phase, up to 2000–3000 ppm O [25,26]. This initial oxygen level in the metal droplets is sourced from the decomposition of less stable oxides at high temperatures prevailing in the arc cavity, and so flux chemistry is used to manage oxygen transfer to the weld metal from the plasma arc [16].

To the authors' knowledge there is no published predictive model for the quantity of oxygen transferred from the gas phase to the weld metal in SAW. The critical importance of such a predictive calculation is to be able to link flux formulations to accurate predictions of oxygen levels in the weld metal, since weld pool element transfer reactions are considered steel deoxidation reactions between slag and metal, and are required to refine weld pool steel to the final weld metal composition [3–6].

The objective of this work is to develop a FactSage (FS) based thermochemical simulation model to predict the end-point steel analysis (weld metal) for a set of material inputs consisting of flux, wire and base plate chemistries, and their proportions. Welding parameters of voltage, current, and welding speed set the energy input level and may be represented in the model by the effective chemical reaction equilibrium temperature as specified in previous studies [3,4,14–16]. Such a simulation model will save time in the specification of weld consumable combinations to attain specific weld metal chemistries associated with oxide inclusion engineering to improve weld metal mechanical properties via acicular ferrite formation [27–29].

## 2. Material and methods

SAW welding tests were made as bead-on-plate runs onto a 350 mm steel plate length, plate thickness was 12 mm and the plate width was 300 mm. The plate dimensions allowed for two parallel runs onto each plate to generate a reserve sample from the second run. Weld heat input was 2.0 kJ/mm (500 A, 28 V, 42 cm/min) and one comparatively lower heat input test at 1.5 kJ/mm (450 A, 30 V, 53 cm/min) welded DCEP (Direct Current Electrode Positive) with 3.2 mm diameter wire.

**Table 2 – Flux compositions (mass%).**

Flux	1	2	3	4	5
MnO	0.87	5.83	1.11	6.80	12.30
CaO	24.20	19.90	25.30	12.50	5.27
Al <sub>2</sub> O <sub>3</sub>	13.90	17.30	17.90	24.90	36.0
SiO <sub>2</sub>	15.10	21.30	13.40	19.60	18.60
MgO	32.10	21.20	29.80	22.20	4.94
Fe <sub>2</sub> O <sub>3</sub>	0.65	1.01	1.10	2.67	5.97
TiO <sub>2</sub>	0.74	1.86	1.18	0.97	10.70
ZrO <sub>2</sub>	0.01	0.01	0.03	0.02	0.24
Na <sub>2</sub> O	2.00	2.69	1.57	1.61	2.20
K <sub>2</sub> O	0.78	1.50	1.15	0.18	0.51
P	0.018	0.031	0.015	0.025	0.033
S	0.033	0.028	0.013	0.018	0.020
F	12.5	11.0	12.6	8.41	2.04
Ba	0.070	0.081	0.017	0.037	0.048
Cr	0.011	0.015	0.010	0.026	0.073
Cu	0.008	0.008	0.005	0.007	0.011
Ni	0.021	0.011	0.003	0.010	0.022
Sr	0.023	0.053	0.006	0.006	0.010
V	0.012	0.013	0.008	0.011	0.031
Moisture	0.020	0.040	0.020	0.000	0.000
Total	103.2	103.9	105.6	100.1	99.1
BI*	3.0	1.8	2.9	1.4	0.5

\* BI calculated from Eq. (1), compound quantities in mass%, [3].

**Table 3 – Crystalline phases present in flux (mass%).**

		Fluoride Basic	Aluminate Basic	Fluoride Basic	Aluminate Basic	Aluminate Rutile
		1	2	3	4	5
Fluorite	CaF <sub>2</sub>	36.6	32.0	29.5	21.7	3.2
Corundum	Al <sub>2</sub> O <sub>3</sub>	24.6	17.2	16.6	20.2	54.4
Periclase	MgO	32.8	36.6	41.1	33.3	7.7
Calcite	CaCO <sub>3</sub>	0	1.3	3.2	0	0
Wollastonite	CaSiO <sub>3</sub>	3.3	8.4	6.1	0	4.4
Mullite	Al <sub>4.52</sub> O <sub>9.74</sub> Si <sub>1.48</sub>	0	0	1.4	17.4	7.3
Quartz	SiO <sub>2</sub>	1.3	1.3	2.1	1.5	2.7
Cristobalite	SiO <sub>2</sub>	0	0	0	1.8	0
Kyanite	Al <sub>2</sub> O <sub>5</sub> SiO <sub>2</sub>	0	0	0	4.1	0
Jacobsite	Fe <sub>2</sub> MnO <sub>4</sub>	0	0	0	0	2.2
Manganosite	MnO	0	0	0	0	1.6
Mn	Mn	0	0	0	0	3.1
Zircon	ZrSiO <sub>4</sub>	0	0	0	0	4.3
Rutile	TiO <sub>2</sub>	1.3	0.3	0	0	9.1
Forsterite	Mg <sub>1.834</sub> Fe <sub>0.155</sub> Ni <sub>0.011</sub> SiO <sub>4</sub>	0	2.9	0	0	0
<b>BI</b>		<b>3.0</b>	<b>1.8</b>	<b>2.9</b>	<b>1.4</b>	<b>0.5</b>

## 2.1. Input materials

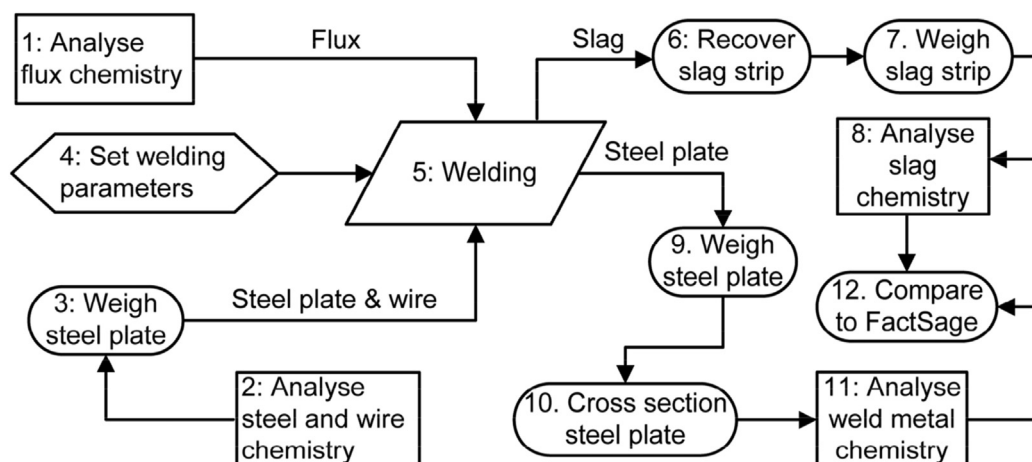
Structural steel grade EN 10025-2 was used as base plate material, as supplied by Xinyu Iron & Steel Co. Ltd., China. The chemical analyses of the weld wire and steel plate are summarised in Table 1. The weld wire major element levels are from the supplier's specification sheet as supplied by Afrox Ltd., South-Africa. The rest of the element analyses in Table 1 were obtained from laboratory analyses.

Five commercial agglomerated fluxes were selected to span a wide range of basicity values (0.5–3.0), and to yield a wide range of weld metal oxygen in the welding test results. The bulk chemical compositions of the fluxes are summarised in Table 2 and XRD (X-ray diffraction) analyses in Table 3. The XRD analyses were done to confirm that the crystalline phases in the flux may be approximated by simplified compound formulas in the FactSage model. For example, fluoride may be added as different crystalline phases besides only CaF<sub>2</sub>. The bulk chemistry analyses only provide the fluorine element mass percentage in the flux, and not the quantity of crystalline compound containing the fluoride addition. Details of the

analyses methods are discussed in section 2.3. According to commercial classification names used in the suppliers' specification sheets, fluxes 1 and 3 are Fluoride Basic fluxes, fluxes 2 and 4 are Aluminate Basic fluxes, and flux 5 is an Aluminate Rutile flux. These classification names and chemistries are in agreement with reported classification names [30].

## 2.2. Experimental procedure

The sequence of experimental steps followed in each welding test is illustrated in Fig. 1. The following description refers to the step numbers in Fig. 1. Input material analyses were done before the welding tests were started (steps 1 and 2). The welding parameters of voltage, current, and welding speed were selected after initial runs were made using flux 1 to attain 1.5 and 2.0 kJ/mm, respectively (step 4). The steel plate mass was measured before and after welding to calculate the quantity of weld wire added to the plate (steps 3 and 9). The weld slag strips from the two weld runs were collected (step 6), cleaned of excess unreacted flux and individually weighed (step 7). Slag strip from the first weld run was chemically

**Fig. 1 – Experimental steps used in each welding test.**

**Table 4 – Real weld metal measurements and delta values (Weld metal composition-Nominal composition) (mass%); #WM=Weld Metal, \*ppm.**

Flux	1	1	1	1	2	2	3	3	4	4	5	5
	#WM	Delta	WM	Delta								
kJ/mm	1.5	1.5	2.0	2.0	2.0	2.0	2.0	2.0	2.0	2.0	2.0	2.0
C	0.110	-0.004	0.110	-0.004	0.100	-0.013	0.100	-0.014	0.110	-0.003	0.100	-0.013
*O	400	374	296	270	377	358	437	411	499	480	687	659
Si	0.130	-0.014	0.170	0.026	0.210	0.068	0.140	-0.004	0.260	0.118	0.650	0.508
Mn	1.060	-0.057	1.140	0.023	1.390	0.305	1.050	-0.067	1.300	0.215	1.480	0.395
*Al	330	88	280	38	240	59	280	38	320	139	470	181
*P	200	75	200	75	230	114	190	65	220	104	270	154
*S	110	-62	100	-72	130	-56	90	-82	110	-76	120	-66
*Ti	50	32	50	32	50	36	50	32	50	36	290	276
Cu	0.100	0	0.100	0	0.110	0	0.100	0	0.110	0	0.110	0

analysed (step 8). The weld metal was analysed after cross sectioning the plate in the middle of the weld length (steps 10 and 11). Details of the sample extraction and analyses methods are discussed in section 2.3. The weld metal and slag analyses are used for comparison to the FactSage model outputs (step 12) as discussed in section 3.2.

### 2.3. Analyses methods

The base plate steel was analysed by optical emission spectroscopy (OES). The oxygen content in the base plate and weld wire was analysed by combustion method. The welded plate was sectioned to remove cross section samples of the weld metal for major element analysis by OES, and total oxygen content analyses by combustion method.

Fluxes and slags were analysed for bulk chemistry by using inductively coupled plasma optical emission spectrometry (ICP-OES), titration method for fluorine analyses, and combustion analysis (LECO) for carbon and sulphur content. Fluxes were also analysed by XRD (X-ray diffraction) to determine which crystalline phases are present in the fluxes. The XRD samples were prepared according to the method described in detail elsewhere [38].

## 3. Results and discussion

### 3.1. Slag and metal analyses

Weld metal analyses are summarised in Table 4. Delta values in Table 4 are defined as the mass% element in weld metal minus the mass% element in the nominal composition, and were calculated from the weld dilution ratio. Dilution ratios were calculated by using the Cu mass balance. The weld metal analyses confirm significant Mn gains when welding with fluxes 2, 4 and 5 and a slight gain or loss of Mn for the rest of the fluxes. Only in the case of fluxes 4 and 5 has the Si level increased significantly. The level of Ti in the weld metal of flux 5 increased by a significant level, from 50 to 290 ppm Ti. Al increased in the weld metal formed from each flux, with the maximum increases for fluxes 4 and 5 (139 and 181 ppm Al).

The slag analyses are summarised in Table 5, and are compared to the unreacted flux analyses. Since F is added to

all these fluxes as CaF<sub>2</sub>, as confirmed in the XRD analyses in Table 3, the following calculation method was used to express the total F analyses in Table 5 as CaF<sub>2</sub>: all F is expressed as CaF<sub>2</sub> and the excess Ca is expressed as CaO. The analyses in Table 5 indicate that the bulk molten slag is chemically similar to its originating flux, although some Fe was added during slag formation. The slag F concentration is decreased somewhat in all tests due to fluoride loss to the gas phase. This loss did not result in a significant change of the BI values. The values of gram slag formed per gram weld wire deposited in the weld metal are displayed in Table 5.

Total weld metal oxygen content vs. flux basicity values for this work are displayed in Fig. 2. The ppm O analysis uncertainty is  $\pm 10$  ppm. Eq. (1) was used to calculate the flux basicity values. The values (dotted line in Fig. 2) generally follow the originally reported trend by Tuliani et al. [24], a decrease in weld metal total oxygen content with increased basicity (solid line in Fig. 2).

The weld metal ppm O levels in this study may be compared to that read from the Tuliani et al. [24] trend line in Fig. 2: flux 1 (BI = 3.0) at 296 ppm O vs. 250 ppm O, flux 2 (BI = 1.8) at 377 ppm O vs. 250 ppm O, flux 3 (BI = 2.9) at 437 ppm O vs. 250 ppm O, flux 4 (BI = 1.4) at 499 ppm O vs. 377 ppm O and flux 5 (BI = 0.5) at 678 ppm O vs. 918 ppm O. The correspondence is not good and the lack of resolution at BI > 1.8 is not helpful.

The levelling out of ppm O at basicity levels in excess of 1.8 does not appear to be confirmed by the data points from this study because at BI > 1.8 the level of ppm O varies from flux to flux. Literature reported values of ppm O at BI > 1.8 varied by as much as  $\pm 100$  ppm O from the constant trend line of 250 ppm O shown in Fig. 2 [14]. Improved resolution in ppm O values in Fig. 2 is required for higher basicity levels (BI > 1.8) to accurately set flux compositions for acicular ferrite formation. The higher level of ppm O for flux 1 at the lower energy input level (1.5 kJ/mm) may be due to shorter weld pool solidification time at lower weld energy input. This shortened time means that less time is available for oxide inclusions to float to the weld pool surface and react with the slag cover layer to exit the liquid steel [5–7].

The extent to which CaF<sub>2</sub> content in the flux influences the level of total oxygen in the weld metal is not easily explained because of the multiple functions of CaF<sub>2</sub> in the flux: hydrogen

**Table 5 – Flux and slag analyses (mass%).**

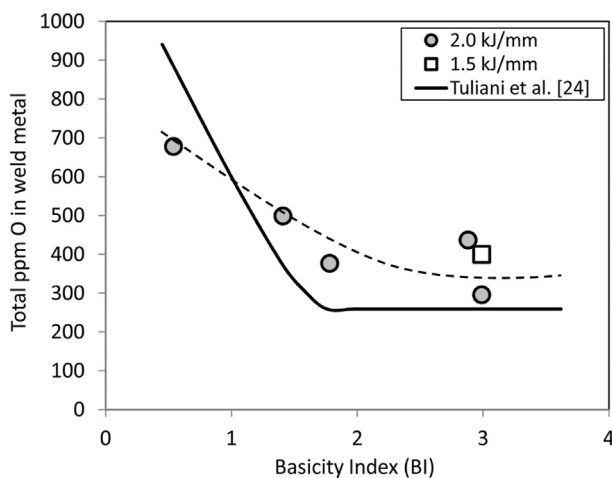
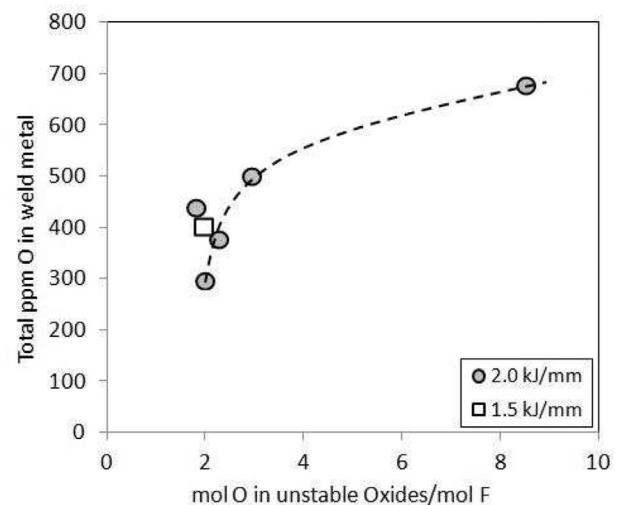
	Flux 1	Slag 1	Slag 1	Flux 2	Slag 2	Flux 3	Slag 3	Flux 4	Slag 4	Flux 5	Slag 5
kJ/mm	1.5	1.5	2.0	2.0	2.0	2.0	2.0	2.0	2.0	2.0	2.0
MnO	0.9	1.3	1.2	5.8	5.5	1.1	1.6	6.8	6.2	12.3	11.5
CaO	5.8	6.6	7.0	3.7	5.7	6.7	7.8	0.1	2.2	2.3	2.9
Al <sub>2</sub> O <sub>3</sub>	13.9	13.2	13.8	17.3	17.4	17.9	16.5	24.9	24.9	36.0	37.7
SiO <sub>2</sub>	15.1	14.5	15.0	21.3	21.1	13.4	12.9	19.6	19.0	18.6	16.6
CaF <sub>2</sub>	25.7	23.2	23.4	22.6	19.5	25.9	23.8	17.9	13.7	4.2	3.6
MgO	32.1	30.4	33.3	21.2	21.6	29.8	28.2	22.2	22.4	4.9	5.2
FeO	0.6	3.2	2.3	0.9	2.7	1.0	3.5	2.4	4.3	5.4	4.8
TiO <sub>2</sub>	0.7	0.7	0.7	1.9	1.8	1.2	1.1	1.0	1.0	10.7	10.9
ZrO <sub>2</sub>	0.0	0.0	0.0	0.0	0.0	0.0	0.0	0.0	0.1	0.2	2.0
Na <sub>2</sub> O	2.0	1.7	1.5	2.7	2.3	1.6	1.4	1.6	2.1	2.2	2.1
K <sub>2</sub> O	0.8	0.8	0.7	1.5	1.4	1.2	1.0	0.2	0.2	0.5	0.5
Total	97.6	95.6	98.9	98.9	99.0	99.8	98.4	96.7	96.1	97.3	97.8
BI	3.0	3.0	3.0	1.8	1.8	2.9	3.0	1.4	1.4	0.5	0.5
g. slag/g. weld wire		0.94		1.02		1.07		0.99		0.89	
Mass% weld wire in weld metal		64		73		64		73		73	

control, slag viscosity control, lowering of the slag solidus and liquidus temperatures and serving as a diluent for unstable oxides which are the source of oxygen from the slag. Furthermore, CaF<sub>2</sub> is also included in the BI index and alternative basicity indexes, such as optical basicity. Therefore, these basicity indexes result in unclear indicator methods of the effect of CaF<sub>2</sub> in the flux on weld metal total oxygen content.

An improved expression of the role of CaF<sub>2</sub> in SAW, or indeed any F<sup>-</sup> source, may be used to express the mol ratio of unstable oxygen to F<sup>-</sup>. This is because the oxygen from unstable oxides (MnO, SiO<sub>2</sub>, MgO) is released in the arc cavity as these oxides are decomposed and this oxygen may be replaced by F<sup>-</sup> ions in the gas phase, and subsequently also in the slag phase. This freed up oxygen is carried by the molten wire droplets into the weld pool and may form oxide inclusions in the weld metal [20,25,26]. Such a plot is shown in Fig. 3 to provide trend information on the effect of CaF<sub>2</sub> content in the flux on the level of total oxygen measured in the weld metal. The use of MnO, SiO<sub>2</sub>, and MgO in the expression as the sources of oxygen is based on welding tests made with

binary CaF<sub>2</sub>-oxide flux mixtures that determined the sequence of oxide stability in the welding arc: CaO, K<sub>2</sub>O, Na<sub>2</sub>O and TiO<sub>2</sub>, Al<sub>2</sub>O<sub>3</sub>, MgO, SiO<sub>2</sub> and MnO [20]. The analysed uncertainty levels for the quantities expressed in the x-axis parameter values in Fig. 3 are ±0.08 mass% for F, ±0.07 mass% for MnO, ±0.29 mass% for SiO<sub>2</sub> and ±0.48 mass% for MgO. From these uncertainty values, the maximum variability in the x-axis parameter in Fig. 3 is calculated as 0.05, 0.05, 0.04, 0.08 and 0.52 for fluxes 1 to 5. The data plot presented in Fig. 3 may be useful to better characterise flux composition vs. weld metal ppm O in fluoride containing fluxes. The anion charge stoichiometric replacement ratio of 2 mol of F<sup>-</sup> for each mol of O<sup>2-</sup> from the unstable oxides (MnO, SiO<sub>2</sub>, MgO) may be an important limit. This plot seems to provide more room for trend resolution at higher fluoride content as compared to the constant ppm O vs. BI trend by Tuliani et al. [24], see in Fig. 2.

Slag FeO content increases with increased weld metal ppm O, as displayed in Fig. 4. This trend is in agreement with previous studies [5,15,33,34]. Excessive levels of oxygen are added

**Fig. 2 – Weld metal total oxygen content vs. flux Basicity Index.****Fig. 3 – (mol O from MnO, SiO<sub>2</sub> and MgO)/mol F in Flux vs. Weld metal Total oxygen content.**

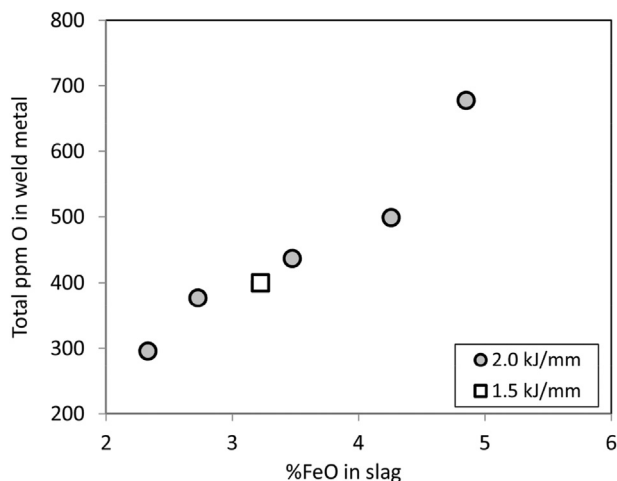


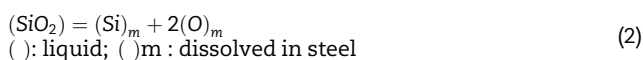
Fig. 4 – Weld metal total oxygen content vs. %FeO in slag.

to the metal droplets that formed from weld wire melted in the arc cavity [25,26]. This initial oxygen level in the metal droplets is influenced by flux chemistry since more oxidising fluxes contain more unstable oxides and less CaF<sub>2</sub>. The consequence is increased levels of oxygen in the metal droplets, up to 3000 ppm O, as the flux decomposes in the arc cavity [25,26]. A large portion of this excess oxygen in the weld pool reacts with the Fe to form FeO in the slag [5,15,33,34]. The excess oxygen is the oxygen in excess of the maximum of 900 ppm O typically present in weld metals as indicated in Fig. 2 for the trend line from Tuliani et al. [24].

### 3.2. Thermochemical simulation results

#### 3.2.1. Basis for thermochemical equilibrium calculations in SAW

Thermodynamic calculations and models were extensively applied in the simulation of SAW [3,14–16,21]. Thermodynamic equilibrium-based calculations are normally used to predict the weld metal C, Si and Mn content for a set of consumables and steel plate. These calculations are not exact in their prediction of weld metal composition without addition of an adjustment factor, but the trend of element addition or loss is usually accurately calculated from equilibrium calculations [3,33–37]. The weld metal ppm O was not calculated in previously reported models. The past approach was to use the empirical relationship of weld metal ppm O vs. flux BI as established by Tuliani et al. [24] to specify the weld metal ppm O as an input value to the equilibrium calculations. Then the equilibrium element content in the weld metal was calculated from the Gibbs energy (reaction equilibrium constant) of the element transfer reaction. For example, see Eq. (2) below for the transfer of Si to the weld metal. If the activity of SiO<sub>2</sub> and the ppm O in the weld metal are specified, the resultant equilibrium Si content in steel can be calculated from the reaction equilibrium constant at the effective SAW reaction equilibrium temperature of 2273 K (2000 °C) [3].



The above approach is useful in setting reaction constraints in the SAW process. However, since ppm O is not calculated, this approach is inadequate to model the process metallurgy of the SAW process. The following reasons were put forward in previous studies to explain why the use of chemical equilibrium of the slag and weld metal is applicable in SAW:

- (a) The effective temperature of chemical reactions in the weld pool is 2000 °C. Firstly, this conclusion is based on thermocouple measurements of the weld pool temperature as a maximum temperature of 2000 °C [3]. Secondly, the effective thermodynamic equilibrium temperature for chemical reactions in SAW was calculated to be 2000 °C for Mn and Si element transfer reactions such as the reaction in Eq. (2). The analysed flux and weld metal compositions were used as inputs to perform this calculation [3].
- (b) Despite large temperature and density gradients among multiple phases (metal, slag and plasma), and the relatively short reaction times in SAW, the assumption can be made that thermodynamic equilibrium is attained locally due to the high temperatures and the high surface-to-volume ratio of reacting phases [16].

Based on the above positive motivational reasons for using thermodynamics to describe the process metallurgy of the SAW process, the following sections discuss the FactSage based gas-slag-metal thermochemical model developed in this work.

#### 3.2.2. Weld metal analyses vs. FactSage calculated weld metal compositions

The welding process was simulated as an equilibrium reactor of gas, slag and weld metal. This simulation approach was also used in a separate study to explain the behaviour of flux TiO<sub>2</sub> in SAW [31]. Here, the experimentally determined mass

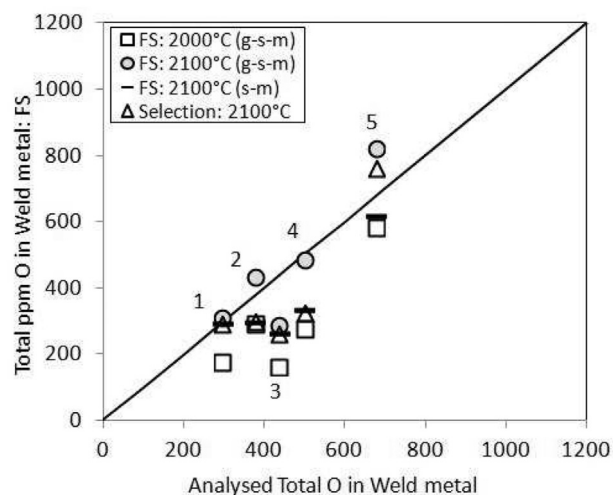


Fig. 5 – Total ppm O in Weld metal: Real vs. FactSage calculated values. (g-s-m: gas-slag-metal equilibrium; s-m: slag-metal equilibrium).

proportions of slag, base plate and wire were used as inputs to the Equilib module in FactSage 7.3. The FToxid, FSstel and FactPS databases were selected and gas phase formation enabled [32]. The flux, base plate and wire compositions from Tables 1 and 5 were used as composition inputs. The equilibration temperature of 2273 K (2000 °C) was initially selected as the equilibration temperature since this is an accepted value stated in literature [3,4,6]. Initial FactSage 6.4 simulation results at 2273 K (2000 °C) were acceptable. In this work FactSage 7.3 is used for 2273 K (2000 °C) and 2373 K (2100 °C), with simulation results at 2373 K (2100 °C) providing the best fit to the measured data.

Comparison of measured weld metal oxygen to the FactSage calculated values at 2273 K (2000 °C) and 2373 K (2100 °C) are illustrated in Fig. 5. Both gas-slag-metal (g-s-m) and the slag-metal (s-m) equilibrium simulations are considered. Oxygen values from the s-m equilibrium calculations correspond to those of the g-s-m equilibrium calculations for flux 1 and 3. As shown in Table 6, this correspondence is due to low levels of gas components formed from fluxes 1 and 3 at analysed weld metal oxygen contents of 296 ppm O and 437 ppm O, respectively. It is clear from Fig. 5 that the calculation results are sensitive to relatively small temperature differences of only 100 K. The calculated gas quantities increased with increased simulation temperature, and the proportion of major gas species changed somewhat, whilst the gas phase partial oxygen pressure remained similar, see Tables 6 and 7.

Although there is some intersection of the calculated s-m and g-s-m values of ppm O in Fig. 5, large differences exist for s-m calculations at 2373 K (2100 °C) for fluxes 2, 4 and 5. Therefore, to accurately simulate the effect of flux chemistry on oxygen transfer to the weld metal the simulation model must be based on g-s-m equilibrium calculations, and not only s-m equilibrium calculations. The data series, Selection: 2100 °C, represents gas-slag-metal equilibria recalculated for 2100 °C with specification of gas species as CO, SiF<sub>4</sub>, NaF and KF only. This selection is discussed in section 3.2.4. In Fig. 5 the calculated oxygen values in this series match the s-m equilibrium values closely for fluxes 1 to 4.

In terms of kinetics, the weld pool solidification time may also influence the weld metal oxygen content since it sets the time available for oxide inclusions to float to the surface of the weld pool and react with the slag cover layer to exit the liquid

steel [5,6]. The weld metal solidification time was calculated from the weld ripple lag distance and welding speed at 4.1–4.7 s. These values are similar to the time calculated from Rosenthal's equation which is dependant on gross heat input as set by voltage, current, welding speed [7]. Therefore, the differences measured in element transfer extent with the use of different fluxes in this series of weld tests are related to chemical and temperature effects only.

Figure 6 (a) illustrates that the calculated weld metal Mn values are within 0.40 mass% of the measured values for gas-slag-metal equilibrium at 2100 °C. This highest absolute difference prevails for flux 5, and the calculated values for fluxes 1 to 4 are closer to the measured values (within 0.15 mass%). In Fig. 6 (b) the calculated mass% Si for fluxes 1 to 3 are within 0.1 mass% of the measured values. For fluxes 4 and 5, the Si values are under-predicted by 0.15 mass% and 0.52 mass%, respectively. Although some Mn is lost to the gas phase as Mn(g) and MnF<sub>2</sub>(g) and Si as SiF<sub>4</sub>(g) and SiO(g), the gas-slag-metal equilibrium calculations indicate these to be less than 2 volume% for the fluxes in this study (see Table 7). Also, the model calculated values for Mn and Si in the weld metal are both, higher and lower relative to the measured weld metal values. Therefore, there is no systematic under or over-prediction of element volatilisation in the gas-slag-metal equilibrium calculation. Activity values of the oxides and fluorides are likely the reason for the differences in calculated and measured Mn and Si values in the weld metal. Higher activities of MnO and SiO<sub>2</sub> in the slag phase result in higher Mn and Si in the weld metal. It is plausible that the activity values of MnO and SiO<sub>2</sub>, and the associated fluorides of Si and Mn, are somewhat inaccurate for the high temperature used in the model (2100 °C). Oxide activity values are extrapolated from lower temperature measurements made in laboratory equilibrium experiments (1600 °C) [3]. In addition, the slag solution models used in FactSage are mathematical approximations of oxide-fluoride slag mixture thermodynamic data, since limited experimentally measured activity data is available [32].

Table 8 provides a comparison of weld metal element analyses to the FactSage calculated values (gas-slag-metal equilibrium) at 2273 K (2000 °C) and 2373 K (2100 °C) for the rest of the weld metal elements. It is well known that weld metal carbon content is close to the nominal composition, with little loss of carbon from oxidation and limited addition of carbon from the weld wire [6,35]. This effect is also observed in our work, the nominal composition is 0.113–0.114 %C vs. real %C analysed at 0.100–0.110 %C. FactSage under-predicted the real weld metal %C in all instances as indicated in Table 8.

The differences between calculated and real Al values in the weld metal differs widely with significant under-prediction for flux 5 and over-prediction for fluxes 1 and 3. In the case of Ti, the FactSage calculations under-predicted the real final weld metal content, although only flux 5 achieved a large delta value for Ti as illustrated in Table 4. The differences between calculated and real values of Al and Ti in weld metal from flux 5 are large, possibly indicating the importance of metallic deoxidation and alloying elements. FactSage over-predicted the weld real metal sulphur content and under-predicted the phosphorus content. Some refinement of sulphur occurred to attain weld metal sulphur values

**Table 6 – FactSage calculated gas properties and volumes in gas-slag-metal equilibrium.**

Flux	K	mass% F to gas	g. gas/ 100 g. Flux	Litre gas/ 100 g. Flux	g./ cm <sup>3</sup>	P <sub>O<sub>2</sub></sub> (atm)
1	2273	4	2	6	1.99E-4	1.30E-10
1	2373	8	4	18	2.02E-4	7.75E-10
2	2308*	38	9	25	3.51E-4	1.58E-9
2	2373	48	11	35	3.20E-4	5.30E-9
3	2273	5	2	10	2.31E-4	1.36E-10
3	2373	12	4	19	2.32E-4	7.97E-10
4	2273	40	6	16	3.90E-4	1.26E-9
4	2373	54	9	26	3.40E-4	7.23E-9
5	2273	91	4	9	4.18E-4	8.86E-9
5	2373	91	4	11	3.69E-4	3.32E-8

\* Calculation did not converge at 2273 K.

**Table 7 – FactSage calculated gas composition in gas-slag-metal equilibrium (volume%).**

Flux	K	CO	Na	K	Mg	NaF	KF	CaF <sub>2</sub>	MgF <sub>2</sub>	MgF	AlF <sub>3</sub>	AlF <sub>2</sub>	NaAlF <sub>4</sub>	TiF <sub>3</sub>	KAlF <sub>4</sub>
1	2273	15	33	10	4	17	12	2	3	2	<1	<1	<1	<1	<1
1	2373	12	29	7	7	17	9	5	6	3	<1	<1	<1	<1	<1
2	2308	8	7	2	<1	17	11	9	13	2	5	2	7	2	9
2	2373	7	8	2	1	17	10	13	16	2	5	2	5	1	5
3	2273	14	22	11	3	15	18	4	4	2	<1	<1	<1	<1	2
3	2373	11	20	8	6	15	13	8	8	4	<1	1	<1	<1	1
4	2273	12	3	<1	<1	9	<1	7	21	2	16	3	16	2	2
4	2373	9	4	<1	1	11	<1	11	25	3	13	4	8	1	1
5	2273	26	1	<1	<1	6	4	<1	1	<1	12	2	8	20	11
5	2373	23	3	<1	<1	9	6	1	1	<1	12	3	6	18	7

\* Calculation did not converge at 2273 K; Not shown: AlF, Mn, MnF<sub>2</sub>, SiF<sub>4</sub>, SiO, and Fe ≤ 2 volume%.

of 90–130 ppm vs. nominal compositions of 172–186 ppm. Phosphorus pick-up occurred since the nominal compositions range is 116–125 ppm vs. the real values of 190–270 ppm.

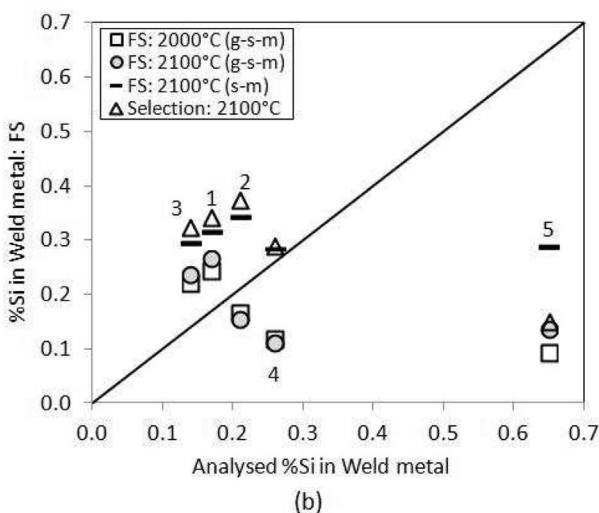
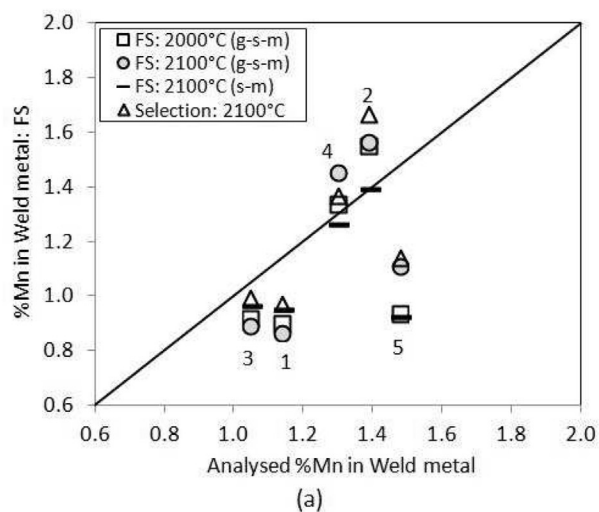


**Fig. 6 – (a): Manganese in weld metal: Real vs. FactSage calculated. (g-s-m: gas-slag-metal equilibrium; s-m: slag-metal equilibrium). (b): Silicon in weld metal: Real vs. FactSage calculated. (g-s-m: gas-slag-metal equilibrium; s-m: slag-metal equilibrium).**

**3.2.3. Post-weld slag analyses vs. FactSage calculated slag compositions**

Figures A1–A11 in Appendix A display the post-weld slag elemental compositions in comparison to the flux chemical analyses, and two sets of model calculated values. The FS: 2100 °C (g-s-m) series are values from the normal unrestricted gas-slag-metal equilibrium calculations and the Selection: 2100 °C series are gas-slag-metal equilibria recalculated with specification of gas species as CO, SiF<sub>4</sub>, NaF and KF. The latter series values are discussed in more detail in section 3.2.4.

The analyses are considered as element values because most of the elements in the slag and flux were chemically analysed as elements, only oxygen is calculated based on the assumption that the oxides are present in the slag as SiO<sub>2</sub>, MnO, Al<sub>2</sub>O<sub>3</sub>, TiO<sub>2</sub>, MgO, CaO, FeO, K<sub>2</sub>O and Na<sub>2</sub>O. FactSage equilibrium slag analyses are stated in terms of a range of fluorides and oxides, with the major oxides as in the above oxygen calculation assumption and predicted fluoride species of NaF, KF, CaF<sub>2</sub>, MgF<sub>2</sub>, FeF<sub>2</sub>, MnF<sub>2</sub>, NiF<sub>2</sub> and CuF. Phase chemistry of the post-weld slag samples were discussed elsewhere and confirm that the slag from fluxes 1 to 5 consisted of a fluoride-oxide liquid mixture at the accepted SAW reaction equilibrium temperature of 2273 K (2000 °C) [38]. Because small quantities of the flux elements are volatilised and even smaller quantities of these elements are transferred between the slag and metal, the shift in the slag composition compared to the flux composition is small. In spite of this, some useful trends may be observed.

Comparison of the flux and slag analyses in Fig. A1 indicates that some fluoride was volatilised in all the fluxes with small quantities volatilised in fluxes 1 and 3, and highest volatilisation levels in fluxes 2 and 4, in agreement with the FactSage numbers for gas formation and composition displayed in Tables 6 and 7. The Si analyses comparison in Fig. A2 shows a loss from the slag relative to the Si level in flux 5. This is expected, considering the delta Si value for flux 5 is high at 0.51 mass% as seen in Table 4. The positive delta Mn values for flux 2, 4 and 5 (see Table 4) did not result in a significant shift in slag Mn composition, Fig. A3. Slag oxygen levels in Fig. A4, as calculated from the assumed cation oxidation states, correspond well for the flux, slag and FactSage simulations, but has limited value given the very small changes of interest in the weld metal oxygen content (300–700 ppm).

**Table 8 – Weld metal compositions: real vs. FactSage (FS) calculated in gas-slag-metal equilibrium.**

Flux	K	%C: Real	%C: FS	ppm Al: Real	ppm Al: FS	ppm Ti: Real	ppm Ti: FS	ppm S: Real	ppm S: FS	ppm P: Real	ppm P: FS
1	2273	0.110	0.055	280	449	50	8	100	173	200	127
1	2373	0.110	0.030	280	596	50	10	100	173	200	126
2	2308*	0.100	0.013	240	153	50	12	130	187	230	117
2	2373	0.100	0.007	240	167	50	12	130	187	230	117
3	2273	0.100	0.051	280	549	50	9	90	173	190	127
3	2373	0.100	0.026	280	743	50	12	90	173	190	126
4	2273	0.110	0.017	320	156	50	4	110	186	220	117
4	2373	0.110	0.008	320	197	50	5	110	186	220	117
5	2273	0.100	0.013	470	57	290	28	120	188	270	117
5	2373	0.100	0.009	470	103	290	46	120	188	270	117

Of higher importance is the Fe content in the slag in Fig. A5, because the level of Fe increased for fluxes 1 to 4, compared to the initial levels in the flux. This is in part due to oxidation of Fe to FeO from reaction of Fe with the excess oxygen entering the weld metal via weld wire molten metal droplets passing through the arc cavity [5,25,26]. For fluxes 1 and 2 the FactSage simulation Fe values are in agreement with the slag analyses, and for fluxes 3 and 4 the FactSage simulation values are placed in between those of the flux and the slag. The Fe level in the slag from flux 5 is slightly lower than in the flux and the FactSage prediction is far higher than either these values, indicating the possible role of deoxidation elements in this flux.

The slag content of major elements, Al, Ti, Mg and Ca, in Figs. A6–A9 remained constant relative to the input flux quantities, and the FactSage simulation results correspond well to the input flux element values. Figure A10 shows that the FactSage calculations over-predicted the volatilisation of K for all the fluxes. In Fig. A11 the slag sodium values for fluxes 1 and 2 are close to the measured values, but the sodium volatilisation extent is under-predicted for fluxes 4 and 5. Calculations from the gas species specification simulations (Selection: 2100 °C) improved only the K volatilisation values for fluxes 1 to 3, but did not improve on the Na volatilisation values as compared to the normal unrestricted gas-slag-metal equilibrium calculations. However, since the quantities of sodium and potassium elements in the fluxes are small at about 1 mass%, the effect on the overall slag analysis is small.

### 3.2.4. Oxygen mass balance and partial oxygen pressure control

Because the formation of FeO in the slag represents a relatively large quantity of oxygen added into the slag, compared to the ppm O added to the weld metal, a simplified oxygen mass balance was calculated to investigate the possible reasons for FeO formation in the slag.

The main source of oxygen in the SAW process is the flux due to dissociation of the flux oxides to oxygen and metal in the plasma arc [20]. Some metallic elements are transferred to the weld metal, typically Si, Mn, Ti and Al, and some elements are evaporated as metallic elements and/or react with CaF<sub>2</sub> to form fluorides such as SiF<sub>4</sub>, NaF and KF. In addition, oxygen may be supplied via CO<sub>2</sub> from the calcination of carbonate in the flux [3,20]. Therefore, the sources of oxygen in the mass balance were calculated as oxygen released due to reduction

of oxides for element transfer to the weld metal and oxygen released in the evaporation of the elements Si, Na and K, known to easily form gaseous fluoride species. Because these elements are sourced from oxides in the flux, the reduction and evaporation steps result in the release of oxygen into the arc column. For flux 3 which contains a significant percentage of carbonate (3 mass%, see Table 3), the oxygen sourced as CO<sub>2</sub> is incorporated into the mass balance. Three oxygen consumption streams were considered, oxygen transferred to the weld metal, oxygen reacted to decarburise the weld metal to form CO gas, and oxygen associated with Fe in the slag as FeO. The results of the oxygen mass balance calculations are summarised in Table 9 and displayed in Fig. 7. It is seen that there is good agreement between the oxygen consumption and supply quantities for fluxes 1 to 4.

The mass numbers for fluxes 1 to 4 illustrate the sensitivity required to accurately apportion some of the gaseous oxygen in the SAW process as oxygen to the weld metal, since the quantity of oxygen released from the flux into the gas phase is orders of magnitude larger than the quantity of oxygen in the solidified weld metal. It appears that oxidation of steel to form FeO in the slag phase plays a major role in oxygen control in the SAW process, even though transfer of oxygen from the flux to the weld metal occurs via the gas phase to the molten weld wire and finally ends up in the weld metal [25,26]. Discrepancy in the oxygen balance for flux 5 (Table 9) is likely due to the presence of deoxidisers in this flux, resulting in an over estimation of the oxygen associated with Si. Even though 3 mass% metallic Mn was identified in the XRD analysis of flux 5 in Table 3, there are likely additional metallic deoxidiser elements present below the detection limit of this technique (2 mass%).

**Table 9 – Oxygen mass balance for welding experiments.**

Flux	1	2	3	4	5
g. O in: Evaporation of SiF <sub>4</sub> , NaF, KF	0.29	0.27	0.04	0.17	0.54
g. O in: Reduction of MnO, SiO <sub>2</sub> , TiO <sub>2</sub> and Al <sub>2</sub> O <sub>3</sub> to weld metal	0.04	0.17	0	0.21	0.64
g. O from CaCO <sub>3</sub> calcination	0	0	0.52	0	0
<b>Total g. O in:</b>	<b>0.33</b>	<b>0.44</b>	<b>0.56</b>	<b>0.37</b>	<b>1.18</b>
g. O out: Oxidation of Fe to FeO	0.22	0.30	0.39	0.30	0
g. O out: O dissolved in weld metal	0.03	0.04	0.04	0.05	0.07
g. O out: O as CO from decarburisation	0.01	0.02	0.02	0.00	0.01
<b>Total g. out:</b>	<b>0.26</b>	<b>0.35</b>	<b>0.45</b>	<b>0.35</b>	<b>0.08</b>

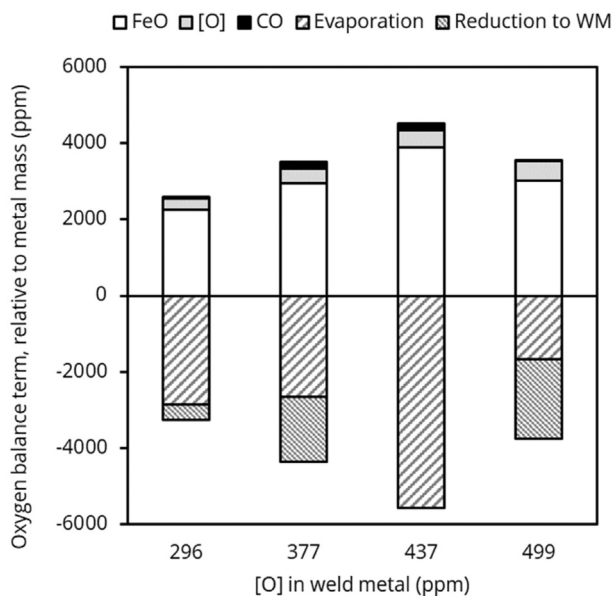
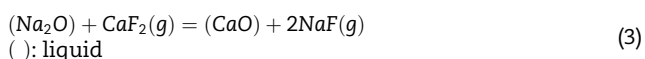


**Fig. 7 – Oxygen mass balance for SAW experiments (ppm O).**

Since the evaporation of Si, Na, and K appear to have a significant influence in the oxygen mass balance numbers in Fig. 7, the speciation of Na and K was further investigated. If Na and K are evaporated as elements rather than fluoride species the expectation is that the oxygen so released in the arc cavity remains as free oxygen to be freely adsorbed onto the molten weld wire droplets and transported into the weld pool. If the Na and K are evaporated as fluoride species via the reaction of the oxide with CaF<sub>2</sub>, see Eq. (3), then the released oxygen from Na<sub>2</sub>O and K<sub>2</sub>O binds to Ca to form CaO which should report to the slag phase. However, one may argue that free oxygen released from the volatilization of Na<sub>2</sub>O and K<sub>2</sub>O will report to the slag as well after oxidising Fe from the weld pool to FeO.



FactSage gas-slag-metal equilibria were recalculated for 2100 °C with specification of gas species as CO, SiF<sub>4</sub>, NaF and KF only. It is seen in Fig. 8(a) that in fluxes 1 to 4 a smaller fraction of flux sodium is volatilised if NaF is specified as the only Na-containing gas species (NaF selection series), compared to the normal unrestricted FactSage simulation of the gas-slag-metal equilibrium, NaF to gas: (g-s-m). For referencing purposes, the Na speciation for the normal unrestricted simulation is summarised in Fig. 8(b), illustrating that a high proportion of Na(g) speciation is expected in the gas phase and smaller quantities of complex fluoride species such as NaAlF<sub>4</sub> (classified as “Other”).

Figure 9(a) and (b) indicate the equivalent values for K. The difference in fraction K volatilised as KF in the two FactSage

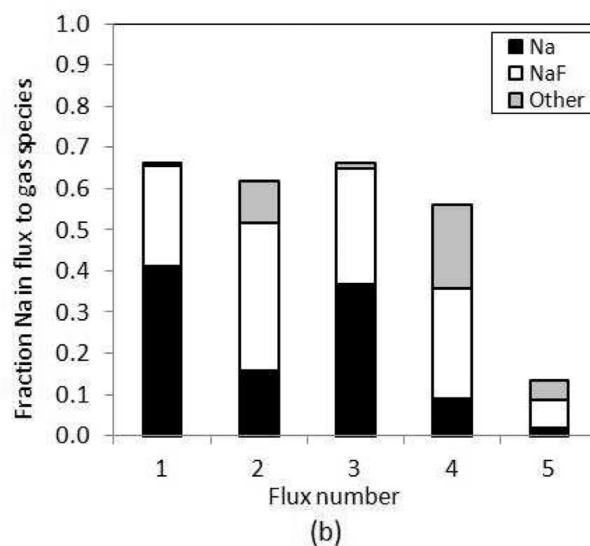
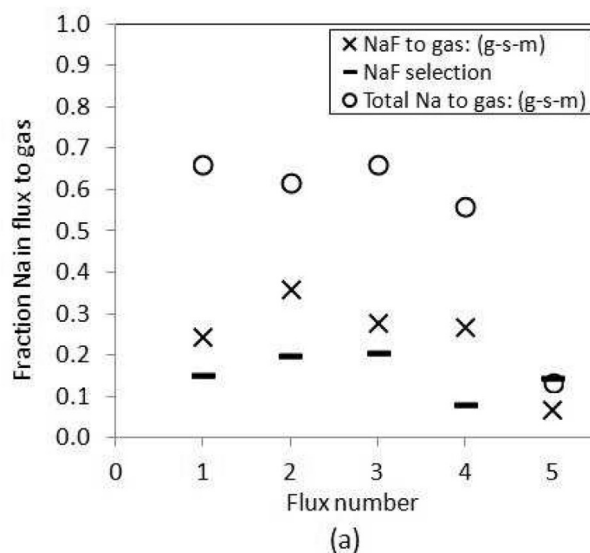


**Fig. 8 – (a): FactSage (gas-slag-metal) calculation scenarios for mass Na to gas at 2373 K. Fig. 8(b): FactSage (gas-slag-metal) Na gas species at 2373 K.**

simulations is similar for fluxes 1 to 3, but large differences exist in the values for fluxes 4 and 5 due to the complex speciation calculation in the normal unrestricted gas-slag-metal equilibrium calculation. Figure 9(b) illustrates that K(g) formation is expected to be proportionally smaller than KF volatilisation, except for flux 4 in which very little KF formation is shown. Figures A1–A11, Appendix A, illustrate the equilibrium slag compositions for the normal unrestricted FactSage simulation of the gas-slag-metal equilibrium and the restricted gas species calculations (Selection: 2100 °C series) in comparison to the analysed post weld slag element

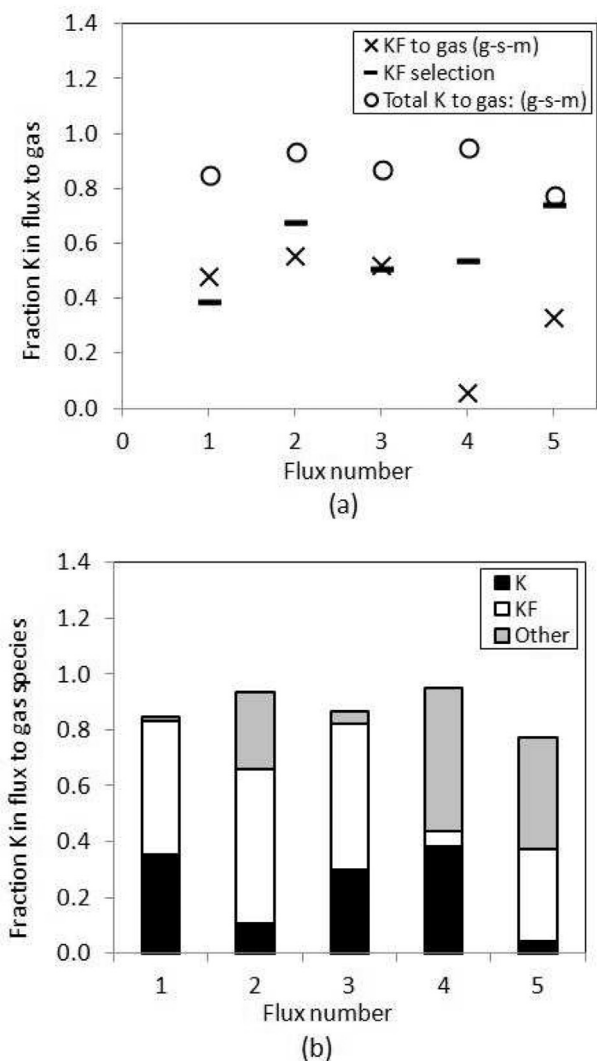


Fig. 9 – (a): FactSage (gas-slag-metal) calculation scenarios for mass K to gas at 2373 K. 9(b): FactSage (gas-slag-metal) K gas species at 2373 K.

composition. Because less K is volatilised as KF alone according to the restricted gas species equilibrium calculation, compared to the normal unrestricted equilibrium calculation, more K is contained in the slag as displayed in Fig. A10, Appendix A. The opposite holds for slag Na content displayed in Fig. A11, Appendix A. For both K and Na content in the slag there is some discrepancy between the analysed slag composition and the equilibrium calculated slag compositions.

To determine if one particular slag-metal reaction controls the weld metal oxygen content, the following thermodynamic calculations were made for individual reactions. The Fe–FeO and Mn–MnO equilibria, reactions in Eq. (4) and Eq. (5) were used to calculate the weld metal oxygen content in

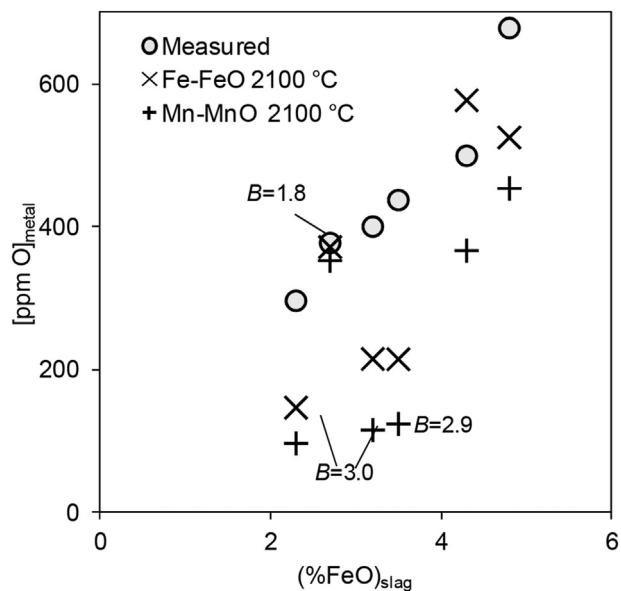


Fig. 10 – ppm O in weld metal: Measured vs. Fe–FeO and Mn–MnO equilibria.

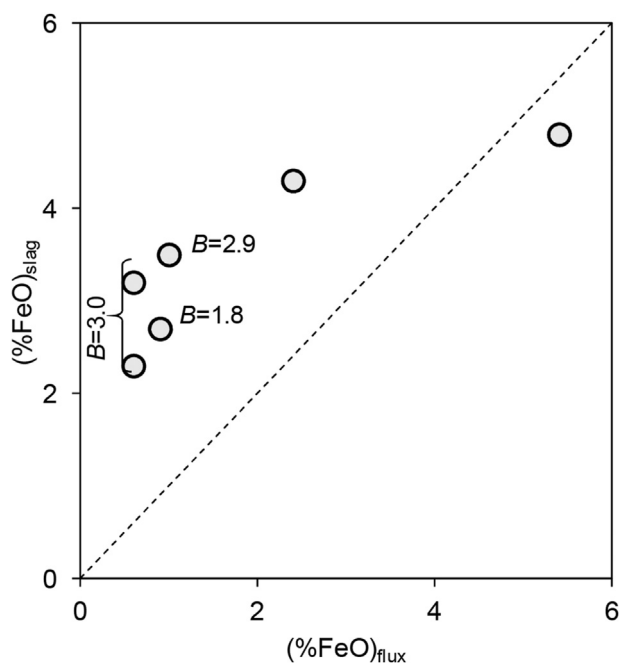
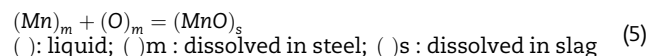


Fig. 11 – mass% FeO: Flux vs. slag.

equilibrium with the weld metal steel and FeO and MnO activities taken from the FactSage simulations. The Gibbs free energy values for the Fe–FeO and Mn–MnO equilibria were taken from literature. The real weld metal Mn composition values from Table 4 were used in these calculations, assuming Henrian behaviour of Mn in steel.



It is generally agreed that the oxidation reaction for Fe proceeds only forward in SAW [5]. Comparison of the calculated equilibrium steel oxygen values for the reactions in Eq. (4) and Eq. (5), to the real measured weld metal oxygen values is illustrated in Fig. 10. It is clear that the weld metal oxygen content is mostly in excess of that expected from the equilibrium values for the reactions in Eqs. (4) and (5). There is correspondence between the real measured ppm O and the equilibrium values for flux 2 only. For the rest of the data points there is a clear systematic positive offset in ppm O values from the Fe–FeO equilibrium trend. From the above analysis one may conclude that the slag FeO content is indeed an indicator of weld metal oxygen content, but it is not useful in any predictive capability since it is not used as a targeted compound in flux formulations.

Comparison of the FeO content in the flux and the slag is illustrated in Fig. 11. It is seen that there is a general trend of increase FeO slag levels with decreasing basicity levels, but this is also not useful in a predictive sense since the BI index is a complex expression. Therefore, the thermochemical simulation calculation method presented here, gas-slag-metal equilibrium for SAW, is an improvement from previous calculations and prediction methods.

In conclusion, comparison of real weld metal and post-weld slag compositions to the calculation results from the FactSage equilibrium simulations indicates that the simulation approach of using gas-slag-metal equilibrium in the FactSage Equilib module has merit. Further refinement and comparison to complete data sets are needed to confirm its application usefulness in saving time in weld consumables specifications.

#### 4. Conclusions

- Weld metal and slag compositions may be predicted from gas-slag-metal thermodynamic equilibrium calculations, provided the flux composition is specified in terms of oxides, fluorides as well as deoxidisers and alloying elements.
- The developed FactSage gas-slag-metal simulation model predicts weld metal ppm O more accurately than the traditionally used empirical trend of BI vs. ppm O.
- The developed FactSage gas-slag-metal model provides resolution of ppm O levels at high flux basicity levels (BI > 1.8), compared to a constant level displayed in the traditionally used empirical trend of BI vs. ppm O.
- Temperature selection is the most important input parameter in obtaining realistic simulation results from the FactSage gas-slag-metal equilibrium calculations.
- Measured weld metal oxygen values appear to follow the calculated Fe–FeO equilibrium trend with a positive offset.

#### Declaration of Competing Interest

The authors declare that they have no known competing financial interests or personal relationships that could have appeared to influence the work reported in this paper.

#### Acknowledgements

This work was supported by the National Research Foundation (NRF) of South Africa [BRIC171211293679].

#### Appendix A. Figures A1–A11

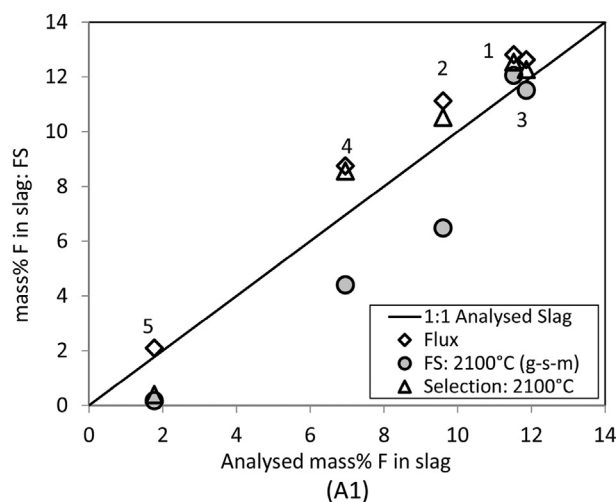


Figure A1 – Slag analyses for F: Real vs. calculated in FactSage gas-slag-metal equilibrium vs. flux input.

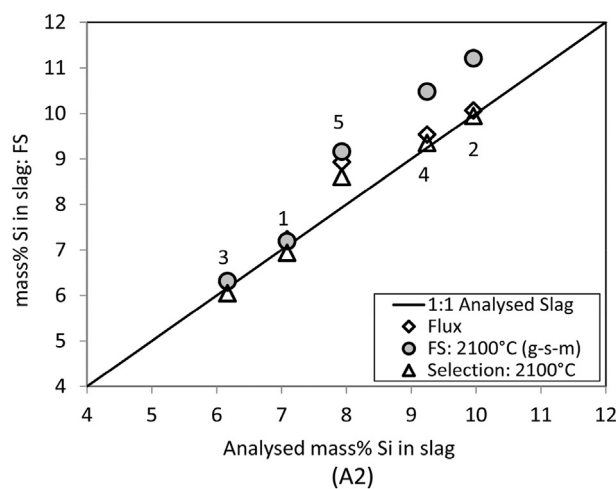


Figure A2 – Slag analyses for Si: Real vs. calculated in FactSage gas-slag-metal equilibrium vs. flux input.

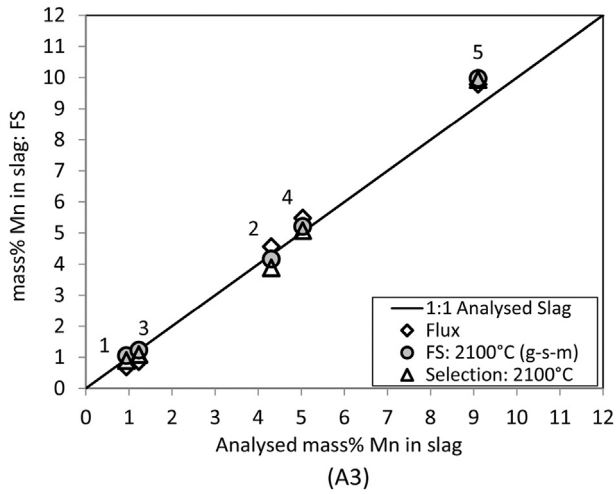


Figure A3 – Slag analyses for Mn: Real vs. calculated in FactSage gas-slag-metal equilibrium vs. flux input.

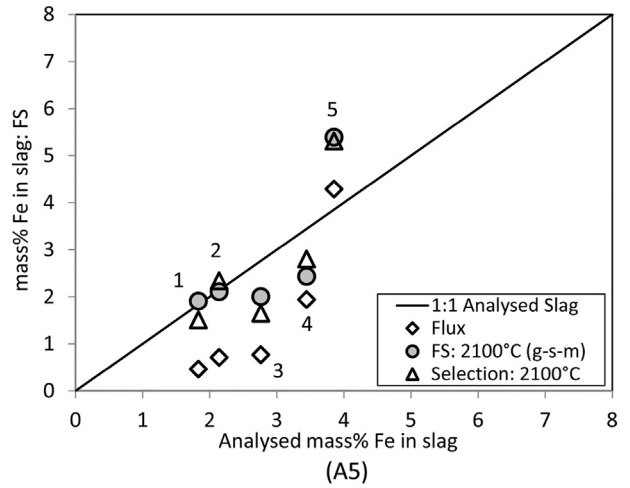


Figure A5 – Slag analyses for Fe: Real vs. calculated in FactSage gas-slag-metal equilibrium vs. flux input.

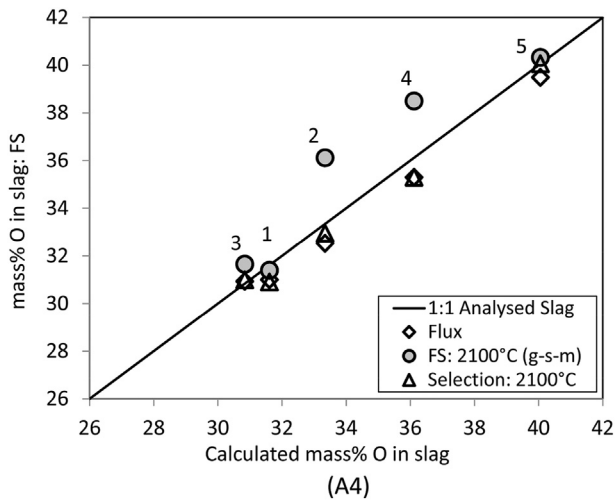


Figure A4 – Slag analyses for O: Real vs. calculated in FactSage gas-slag-metal equilibrium vs. flux input.

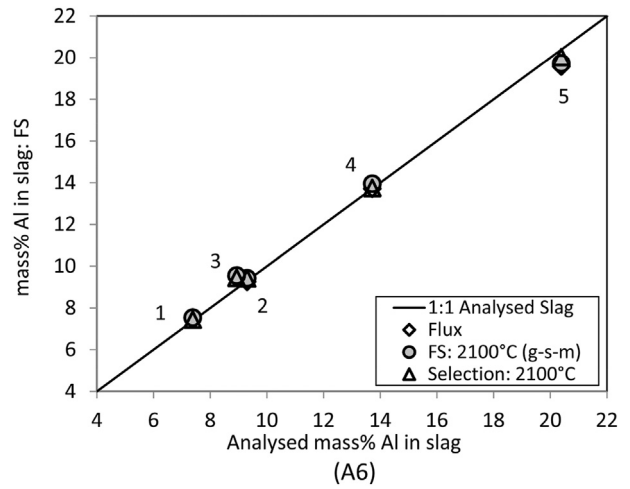


Figure A6 – Slag analyses for Al: Real vs. calculated in FactSage gas-slag-metal equilibrium vs. flux input.

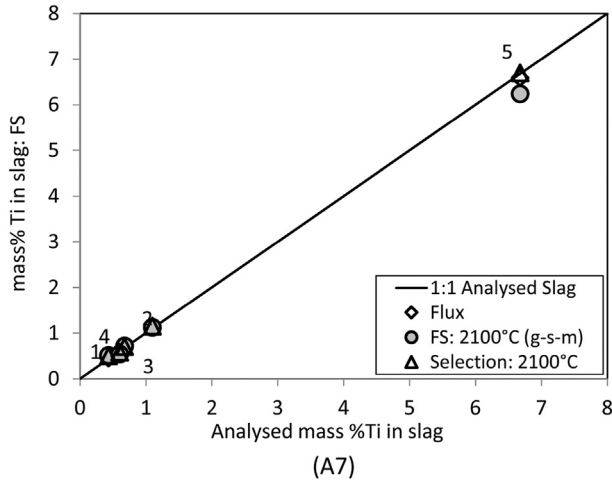


Figure A7 – Slag analyses for Ti: Real vs. calculated in FactSage gas-slag-metal equilibrium vs. flux input.

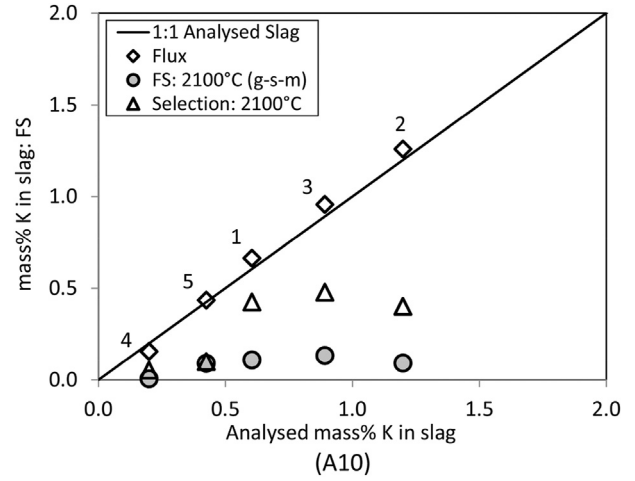


Figure A10 – Slag analyses for K: Real vs. calculated in FactSage gas-slag-metal equilibrium vs. flux input.

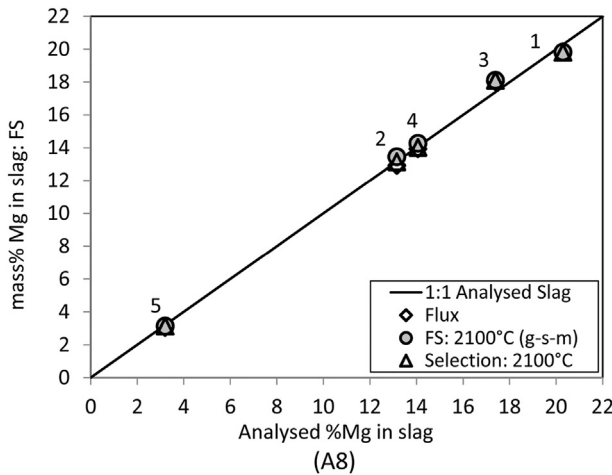


Figure A8 – Slag analyses for Mg: Real vs. calculated in FactSage gas-slag-metal equilibrium vs. flux input.

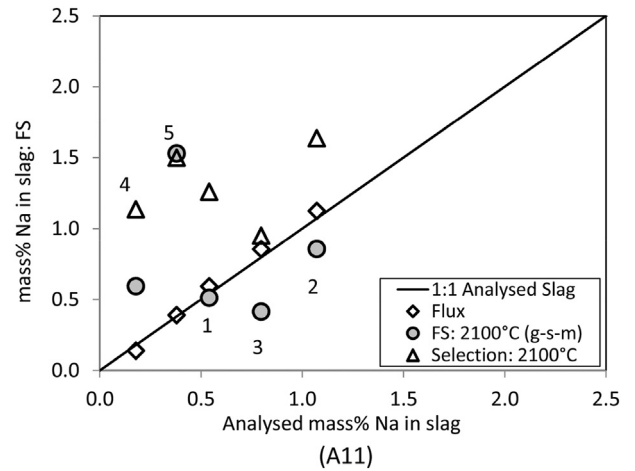


Figure A11 – Slag analyses for Na: Real vs. calculated in FactSage gas-slag-metal equilibrium vs. flux input.

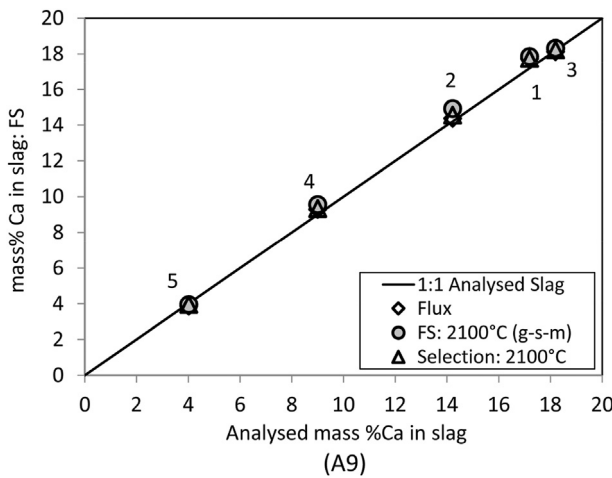


Figure A9 – Slag analyses for Ca: Real vs. calculated in FactSage gas-slag-metal equilibrium vs. flux input.

REFERENCES

- [1] Sengupta V, Havrylov D, Mendez PF. Physical phenomena in the weld zone of submerged arc welding – A Review. *Weld J* 2019;98:283S–313S.
- [2] Biesuz M, Saunders T, Ke D, Reece MJ, Hu C, Grasso S. A review of electromagnetic processing of materials (EPM): heating, sintering, joining and forming. *J Mater Sci Technol* 2021;69:239–72.
- [3] Chai CS, Eagar TW. Slag-metal equilibrium during submerged arc welding. *Metall Trans B* 1981;12:539–47.
- [4] Mitra U, Eagar TW. Slag-metal reactions during welding: part I. Evaluation and reassessment of existing theories. *Metall Trans B* 1991;22:65–71.
- [5] Mitra U, Eagar TW. Slag-metal reactions during welding: part II. Theory. *Metall Trans B* 1991;22:73–81.
- [6] Mitra U, Eagar TW. Slag-metal reactions during welding: part III. Verification of the theory. *Metall Trans B* 1991;22:83–100.

- [7] Klukan AO, Grong Ø. Mechanisms of inclusion formation in Al-Ti-Si-Mn deoxidized steel weld metals. *Metall Trans A* 1989;20:1335–49.
- [8] Dallam CB, Liu S, Olson DL. Flux composition dependence of microstructure and toughness of submerged arc HSLA weldments. *Weld J* 1985;64:140S–52S.
- [9] Paniagua-Mercado AM, Lopez-Hirata VM, Saucedo Munoz ML. Influence of the chemical composition of flux on the microstructure and tensile properties of submerged-arc welds. *J Mater Proc Technol* 2005;169:346–51.
- [10] Kohno R, Takamo T, Mori N, Nagano K. New fluxes of improved weld metal toughness for HSLA steels. *Weld J* 1982;61:373S–80S.
- [11] Bang K, Park C, Jung H, Lee J. Effects of flux composition on the element transfer and mechanical properties of weld metal in submerged arc welding. *J. Met. Mater. Int.* 2009;15:471–7.
- [12] Chai CS, Eagar TW. The effect of SAW parameters on weld metal chemistry. *Weld J* 1980;59:93S–8S.
- [13] Singh B, Khan ZA, Siddiquee AN. Effect of flux composition on element transfer during Submerged Arc Welding (SAW): a literature review. *Int J Curr Res* 2013;5:4181–6.
- [14] Eagar TW. Sources of weld metal oxygen contamination during submerged arc welding. *Weld J* 1978;57:76S–80S.
- [15] Mitra U, Eagar TW. Slag metal reactions during submerged arc welding of alloy steels. *Metall Trans A* 1984;15:217–27.
- [16] Indacochea JE, Blander M, Christensen N, Olson DL. Chemical reactions during submerged arc welding with FeO-MnO-SiO<sub>2</sub> fluxes. *Metall Trans B* 1985;16:237–45.
- [17] Baunè E, Bonnet C, Liu S. Reconsidering the basicity of a FCAW consumable-Part 1: solidified slag composition of a FCAW consumable as a basicity indicator. *Weld J* 2000;79:57S–65S.
- [18] Du Plessis J, Du Toit M, Pistorius PC. Control of diffusible weld metal hydrogen through flux chemistry modification. *Weld J* 2007;86:273S–80S.
- [19] Kim JB, Lee TH, Sohn I. Effect of compositional variation in TiO<sub>2</sub>-based flux-cored arc welding fluxes on the thermo-physical properties and mechanical behavior of a weld zone. *Metall Trans A* 2018;49:2705–20.
- [20] Chai CS, Eagar TW. Slag metal reactions in binary CaF<sub>2</sub>-metal oxide welding fluxes. *Weld J* 1982;61:229S–32S.
- [21] Palm HJ. How fluxes determine the metallurgical properties of submerged arc welds. *Weld J* 1972;51:358S–60S.
- [22] Burck PA, Indacochea JE, Olsen DL. Effects of welding flux additions on 4340 steel weld metal composition. *Weld J* 1990;69:115S–22S.
- [23] Park J-Y, Chang W-S, Sohn I. Effect of MnO to hydrogen dissolution in CaF<sub>2</sub>-CaO-SiO<sub>2</sub> based welding type fluxes. *Sci Technol Weld Join* 2012;17:134–40.
- [24] Tuliani SS, Boniszewski T, Eaton NF. Notch toughness of commercial submerged arc weld metal. *Weld Met Fabr* 1969;37:327–39.
- [25] Polar A, Indacochea JE, Blander M. Electrochemically generated oxygen contamination in submerged arc welding. *Weld J* 1990;69:68S–74S.
- [26] Lau T, Weatherly GC, Mc Lean A. The sources of oxygen and nitrogen contamination in submerged arc welding using CaO-Al<sub>2</sub>O<sub>3</sub> based fluxes. *Weld J* 1985;64:343S–7S.
- [27] Koseki T, Thewlis g. Inclusion assisted microstructure control in C-Mn and low alloy steel welds. *Mat Sci Technol* 2005;21:867–79.
- [28] Sarma DS, Karasev AV, Jonsson PG. On the role of non-metallic inclusions in the nucleation of acicular ferrite in steels. *ISIJ Int* 2009;49:1063–74.
- [29] Loder D, Michelic SK, Mayerhofer A, Bernhard C. On the capability of nonmetallic inclusions to act as nuclei for acicular ferrite in different steel grades. *Metall Trans B* 2017;48:1992–2006.
- [30] Kumar A, Singh H, Maheshwari S. A review study of Submerged Arc Welding fluxes. *i-manager's J Mech Eng* 2013;3:44–52.
- [31] Zhang J, Coetsee T, Basu S, Wang C. Impact of gas formation on the transfer of Ti and O from TiO<sub>2</sub>-bearing basic fluoride fluxes to submerged arc welded metals: a thermodynamic approach. *Calphad* 2020;71:102195. <https://doi.org/10.1016/j.calphad.2020.102195>.
- [32] Bale CW, Bélisle E, Chartrand P, Decterov S, Eriksson G, Gheribi A, et al. Reprint of FactSage thermochemical software and databases. 2010–2016. *CALPHAD* 2016;55:1–19.
- [33] Zhang J, Coetsee T, Wang C. Element transfer behaviors of fused CaF<sub>2</sub>-SiO<sub>2</sub> fluxes subject to high heat input submerged arc welding. *Metall Mater Trans B* 2020;51:16–21.
- [34] Zhang J, Coetsee T, Dong H, Wang C. Element transfer behaviors of fused CaF<sub>2</sub>-SiO<sub>2</sub>-MnO fluxes under high heat input submerged arc welding. *Metall Mater Trans B* 2020;51:885–90.
- [35] Zhang J, Coetsee T, Dong H, Wang C. Elucidating the roles of SiO<sub>2</sub> and MnO upon decarburization during Submerged Arc welding: a thermodynamic study into EH36 shipbuilding steel. *Metall Mater Trans B* 2020;51:1805–12.
- [36] Zhang J, Coetsee T, Dong H, Wang C. Fine-tuned element transfer strategies for ternary CaF<sub>2</sub>-SiO<sub>2</sub>-CaO fluxes in Submerged Arc welding: an environmentally friendly approach. *Metall Mater Trans B* 2020;51:1350–4.
- [37] Zhang J, Coetsee T, Dong H, Wang C. Element transfer behaviors of fused CaF<sub>2</sub>-TiO<sub>2</sub> fluxes in EH36 shipbuilding steel during high heat input Submerged Arc welding. *Metall Mater Trans B* 2020;51:1953–7.
- [38] Coetsee T. Phase chemistry of Submerged Arc Welding (SAW) fluoride based slags. *J Mater Res Technol* 2020;9:9766–76.